Journal of Materials Chemistry

Cite this: J. Mater. Chem., 2012, 22, 1364

www.rsc.org/materials

PAPER

Efficient organic optoelectronics with multilayer structures

Tsung-Hsien Kuo,[ab] Fang-Chung Chen,[c] Juo-Hao Li,[b] Annie Tzuyu Huang,[b] Jen-Hsien Huang,[b] Kuo-Chuan Ho*[ad] and Chih-Wei Chu*[bc]

Received 18th July 2011, Accepted 28th October 2011
DOI: 10.1039/c1jm13373j

In this study we developed efficient polymer solar cells (PSCs) and polymer light emitting diodes (PLEDs) incorporating multilayer structures prepared through solution processing. To prevent dissolution of the bottom layer by the subsequent layer, we used a polydimethylsiloxane stamp to transfer the film onto the target surface. The active layer of the PSCs consisted of a poly(3-hexylthiophene) (P3HT)-rich layer and a [6,6]-phenyl-C_{61}-butyric acid methyl ester (PCBM)-rich layer; the active layer of the PLEDs consisted of a blue-polyfluorene as the light emitting layer (LEL) and poly (9,9-di-*n*-octylfluorene-*alt*-(1,4-phenylene-((4-*sec*-butylphenyl)imino-1,4-phenylene))) (TFB) as the electron blocking layer (EBL). We found that the efficiency of devices was readily manipulated by changing the constitution of each stacking layer. After optimizing the fabrication conditions for each functional layer, we obtained PSCs reaching a power conversion efficiency of 3.52%. The efficiency of PLEDs incorporating an EBL was 27% greater (reaching 4.7 cdA^{-1}) than that prepared without an EBL layer.

Introduction

Organic optoelectronic devices have received a great deal of attention from both industrial and academic research groups because of their ease of fabrication and excellent mechanical properties. Solution-processable organic semiconductors offer particularly attractive routes for the high-throughput, low-cost, and large-area fabrication of such optoelectronic devices as photodectors,[1,2] light emitting diodes (LEDs),[3,4] and solar cells.[5,6] The performance of devices prepared using soluble conjugated organic compounds is limited, however, by their large band gaps and relatively poor transport properties, resulting in weaker performance relative to that of their inorganic counterparts. Recently, white organic LEDs featuring multilayer structures, fabricated through vacuum processing, have reached fluorescent tube efficiency.[7,8] Therefore, one potential solution to fulfilling the increasing demand for devices prepared from soluble conjugated organics is to combine the functionalities of different organic materials in multilayer device structures. Although multilayer structures can provide high-performance optoelectronic devices, solution processing often leads to dissolution of the underlying layers by sequential layers. To overcome this obstacle, many methods have been developed to fabricate multilayer polymer optoelectronics, including thermal lamination,[9] transferring printing,[10,11] and liquid buffer layer method.[12–15] In a previous study, we developed a non-invasive and non-contaminative stamping technique for the fabrication of multilayer structures through solution processing; as a proof-of-concept, we demonstrated the use of this stamping technique to form multilayer polymer structures for use in polymer solar cells.[16]

One of the most promising bulk heterojunction (BHJ) solar cells is that based on P3HT as the donor and PCBM as the acceptor, with power conversion efficiencies (PCEs) approaching 5%.[17] Although the BHJ provides a relatively large interface for exciton dissociation, the efficiency remains limited by carrier recombination in isolated pockets and unfavorable contact between the organics and the electrodes (*e.g.*, donor/cathode and acceptor/anode), due to the random distribution of the donor and acceptor materials in such structures.[18–20] Even when thermal and solvent annealing are applied to control the BHJ morphology and, therefore, eliminate most of the isolated pockets,[21–25] unfavorable contacts remain between the organics and the electrodes, due to the surface energy of P3HT (26.9 mJ m^{-1}) being less than that of PCBM (37.8 mJ m^{-1}).[26] Many groups have reported that the efficiency of devices can be enhanced by incorporating low-surface energy fullerene derivatives in P3HT/PCBM blends.[27,28] These fullerene derivatives can migrate spontaneously to the top of the BHJ active layer during coating, thereby preventing the donor from touching the cathode. Nevertheless, this approach may minimize the surface area of the donor–acceptor junction, and many of the PCBM molecules can

[a]*Institute of Polymer Science and Engineering, National Taiwan University, Taipei, Taiwan, 115. E-mail: gchu@gate.sinica.edu.tw*
[b]*Research Center for Applied Sciences, Academia Sinica, Taipei, Taiwan 115. E-mail: kcho@ntu.edu.tw*
[c]*Department of Photonics, National Chiao-Tung University, Hsinchu, Taiwan 300*
[d]*Department of Chemical Engineering, National Taiwan University, Taipei, Taiwan 106*

remain in contact with the anode. There have also been impressive improvements in the carrier balance of polymer LEDs through molecule design,[29,30] but the efficiency is far behind that of OLEDs because the multilayer structure can easily balance the hole and electron current by incorporating functional layers, such as emissive layer, carrier transport layer, and carrier blocking layer. For these reasons, in this study we employed a multilayer structure, in conjunction with our previously developed stamping technique, to prepare efficient PSCs and PLEDs. To minimize unfavorable contact between the organics and the electrodes in BHJ solar cells, while not significantly shrinking the area of the donor–acceptor junction, we studied bilayer structures incorporating different fractions of P3HT/PCBM blend layers. Furthermore, to balance carrier transport in PLEDs, we studied a bilayer structure incorporating blue-PF as the light emitting layer (LEL) and TFB as the hole transport layer (HTL).

Experimental

PDMS stamps were synthesized from the oligomer Silgard 184A and the curing agent Silgard 184B. The detailed preparation process has been reported previously.[15] The transfer scheme is illustrated in Fig. 1. Initially, the surface of the PDMS stamp was treated with organic solvent, depending on the solvent used to dissolve the polymers (Fig. 1B), and then the polymer film was spun directly onto the PDMS surface (Fig. 1C). The stamping process was then performed by attaching the PDMS stamp coated with the polymer film onto the target surface under thermal and physical driving forces (Fig. 1D).

After cleaning an indium tin oxide (ITO) glass, poly(ethylene dioxythiophene):polystyrenesulfonate (PEDOT-PSS, CLEVIOS™ P) was spin-coated to form a layer having a thickness of 30 nm. BHJ films featuring different fractions of P3HT:PCBM were deposited on the treated PDMS stamp by spin-coating (1500 rpm) chloroform solutions containing different solid contents. Active layers featuring the stacking of two different fractions of P3HT:PCBM blend films were formed through sequential transfer from the PDMS stamp. The active layer of the PLEDs consisted of poly(9,9-di-*n*-octylfluorene-*alt*-(1,4-phenylene-((4-*sec*-butylphenyl)imino-1,4-phenylene)))(TFB), deposited by spin-coating a xylene solution containing 0.5 wt% (w/v) TFB at various spinning rates, and B–PF, deposited on the PDMS stamp by spin-coating a xylene solution containing 0.5 wt% (w/v) B–PF and then transferred onto the TFB layer. Finally, 30 nm thick calcium and 100 nm thick aluminium layers were thermally evaporated under vacuum at a pressure below 6×10^{-6} torr through a shadow mask. The active area of the device was 0.1 cm^2.

The current density–voltage (*J–V*) characteristics of the PLEDs and PSCs were tested using an Agilent 4156C semiconductor parameter analyzer placed within a N_2-filled glove box. The EL efficiency was measured using a Photo Research PR650 spectrophotometer integrated with Alignment 4156C. The photocurrents of the PSCs were tested under simulated AM 1.5 G irradiation (100 mW cm^{-2}) using a Xe lamp-based solar simulator (Thermal Orel 1000 W). The external quantum efficiency (EQE) spectrum was obtained under short-circuit conditions. The effective range of the monochromator was 190–900 nm. The absorption spectra were recorded using a Jasco-V-670 UV-Vis spectrophotometer. The surface morphology of the films was imaged using atomic force microscopy (AFM, digital instrument). X-Ray photoelectron spectroscopy (XPS) was performed using a PHI 5000 VersaProbe (ULVAC-PHI Chigasaki, Japan) system, with a micro-focused (100 em, 25 W) Al X-ray beam and a Wien-filtered + ion source (IOG C60-10, Ionoptika, Chandler's Ford, UK) operated at 10 nA and 10 kV.

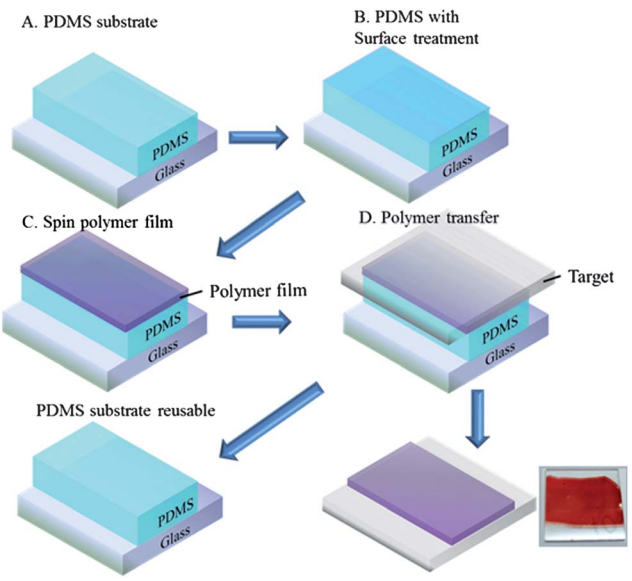

Fig. 1 Schematic representation of the thin film transfer procedure using PDMS substrates. (a) PDMS substrate prepared on the glass substrate; (b) organic solvent spin-coated onto the PDMS surface; (c) polymer film spun onto the PDMS substrate; (d) transfer of the film from the PDMS surface to the target substrate.

Results and discussion

Making the active layer richer in donors and acceptors near the anode and cathode, respectively, will decrease carrier recombination at the metal–organic interface[31] and balance the hole and electron mobilities.[32] To optimize the film morphology in the BHJ, we used a stamping technique to fabricate bilayer PSCs containing a PCBM-rich layer (top layer) and a P3HT-rich layer (bottom layer). Fig. 2(a) presents a schematic representation of

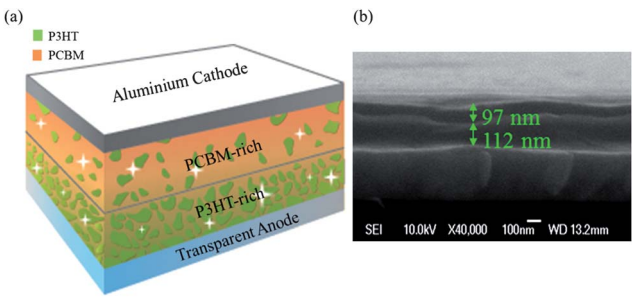

Fig. 2 (a) Schematic representation of the control over the P3HT-rich/PCBM-rich compositions of bilayer structures. (b) Side-view SEM image of a P3HT-rich/PCBM-rich bilayer structure.

the device. The thickness of each layer was 120 nm, as measured by the Alpha-step. Fig. 2(b) displays a cross-sectional SEM image of the bilayer structure on the ITO glass. The interface between the top and bottom layers is clearly evident after the transferring from the PDMS stamp. To determine the influence of the BHJ film morphology in vertical direction on the carrier mobilities and the cell performance, we also constructed PSCs having a bilayer structure with different fractions of P3HT/PCBM blends. The solid contents of P3HT and PCBM in the bilayer active layers were kept constant for all devices to minimize the effects of other factors on device performance. The bottom layer was P3HT:PCBM blended with different weight ratios of P3HT only (1 : 0), 1 : 0.25, 1 : 0.5, and 1 : 1; the composition of the top layer featured weight ratios of 1 : 2, 1 : 1.75, 1 : 1.5, and 1 : 1, so they all add up to 2 : 2. In addition, we also fabricated a single BHJ layer having a P3HT/PCBM ratio of 1 : 1. Fig. 3 presents AFM images of films of various compositions, revealing the interfaces between the bottom and top layers. The printed bottom layer surfaces were fairly flat, with a root-mean-square roughness ranging from 2.3 to 3.5 nm, depending on the P3HT:PCBM ratio. The flat surface of the bottom layer resulted in good contact after transferring the top layer onto the bottom layer through the stamping process.

Because only P3HT contains sulfur atoms, measuring the content of sulfur—through XPS depth profiles—allowed us to determine the concentration gradients within the active layers. Fig. 4 displays XPS depth profiles of the bilayer structures having bottom/top compositions of 1 : 0.25/1 : 1.75 and 1 : 1/1 : 1. For the latter, the sulfur concentration was nearly the same throughout the top and bottom layers. In contrast, for the film featuring bottom/top compositions of 1 : 0.25/1 : 1.75, the atomic concentration of sulfur at the surface of the top layer was 1.2%, but it reached 2.1% after etching through 240 nm of the

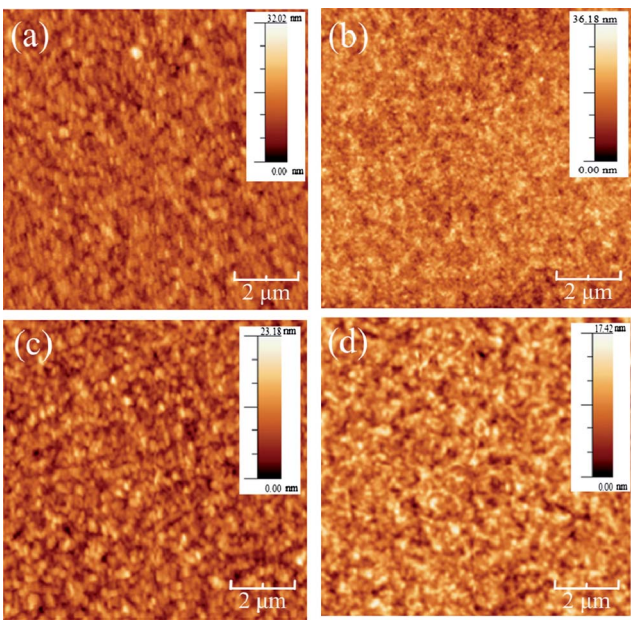

Fig. 3 AFM images of (a) 100% P3HT bottom layer and (b)–(d) P3HT-rich layers with P3HT/PCBM compositions of (b) 1 : 0.25, (c) 1 : 0.5, and (d) 1 : 1. The images were recorded in tapping mode; surface area: 10 × 10 μm^2.

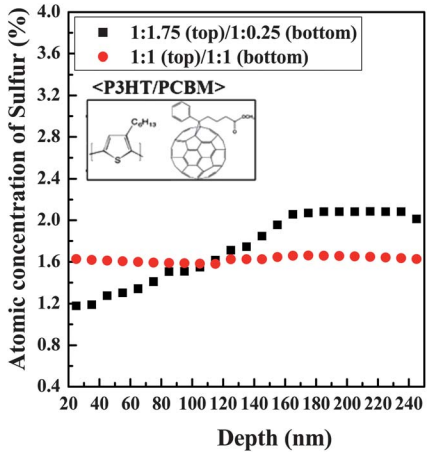

Fig. 4 XPS depth profiles of bilayer structures with (■) the top layer (1 : 1.75 P3HT/PCBM ratio) transferred onto the bottom layer (1 : 0.25 P3HT/PCBM ratio) and (●) the top layer (1 : 1 P3HT/PCBM ratio) transferred onto the bottom layer (1 : 1 P3HT/PCBM ratio).

film. The occurrence of an intermixed zone may have been caused by residual chloroform in the top layer, partially swelling the bottom layer during the stamping transfer process. Thus, enrichment of PCBM on the side of the photoactive layer close to the cathode and enrichment of P3HT close to the anode can be controlled using stamping technology.

Thermal treatment can have a great effect on the performance of OPVs because it strongly affects the crystalline order and phase separation of the photoactive layer, thereby influencing charge carrier transport and collection.[33] To examine the influence of the bilayer film morphology on the charge transport properties, we fabricated hole- and electron-only devices to calculate the hole and electron mobilities by fitting the dark current–voltage (J–V) curves to the space-charge-limited current model.[34] Table 1 lists the calculated electron and hole mobilities for single-layer devices and bilayer devices of various compositions. The hole and electron mobilities of the single BHJ layer device ($\mu_e = 2.16 \times 10^{-7}$ m^2 V^{-1} s^{-1}, $\mu_h = 9.93 \times 10^{-7}$ m^2 V^{-1} s^{-1}) were similar to that of the bilayer device ($\mu_e = 1.79 \times 10^{-7}$ m^2 V^{-1} s^{-1}, $\mu_h = 9.88 \times 10^{-8}$ m^2 V^{-1} s^{-1}) in which the top and bottom layers both featured a 1 : 1 P3HT/PCBM ratio. Thus, the stamping process generates a good contact interface between the top and bottom layers. Although the electron and hole mobilities of other combinations were both lower than that of the single-layer BHJ device, they exhibited a better balance of charge carrier transport. We attribute the lower charge carrier mobilities to enrichment of PCBM on the side of the photoactive layer close to the negative electrode and enrichment of P3HT close to the

Table 1 Hole mobilities, electron mobilities, and hole-to-electron-mobility ratios of devices with BHJ and P3HT/PCBM composition-controlled bilayer structures

Composition of P3HT and PCBM (bottom/top)	Hole mobility μ_h/m^2 V^{-1} s^{-1}	Electron mobility μ_e/m^2 V^{-1} s^{-1}	μ_e/μ_h
1 : 1 (BHJ)	9.93×10^{-8}	2.16×10^{-7}	2.18
1 : 1/1 : 1 (bilayer)	9.88×10^{-8}	1.79×10^{-7}	1.81
1 : 0.5/1 : 1.5 (bilayer)	8.54×10^{-8}	1.21×10^{-7}	1.41
1 : 0.25/1 : 1.75 (bilayer)	7.20×10^{-8}	8.34×10^{-8}	1.16
P3HT only/1 : 2 (bilayer)	6.16×10^{-8}	8.29×10^{-8}	1.34

positive electrode, causing the charge carriers to be collected efficiently by their respective electrodes. For the system in which the top layer had a P3HT/PCBM ratio of 1 : 1.75 and the bottom layer had a ratio of 1 : 0.25, we obtained the most-balanced charge transport ($\mu_e/\mu_h = 1.16$), with electron and hole mobilities of $\mu_e = 8.34 \times 10^{-8}$ m^2 V^{-1} s^{-1} and $\mu_h = 7.20 \times 10^{-8}$ m^2 V^{-1} s^{-1}, respectively.

Fig. 5(a) displays the EQE spectra of bilayer devices featuring different combinations of P3HT and PCBM in their top and bottom layers. The single-layer BHJ device featuring a P3HT/PCBM ratio of 1 : 1 exhibited a maximum EQE of 55%; for the bilayer device in which the bottom layer had a P3HT/PCBM ratio of 1 : 0.25 and the top had a ratio of 1 : 1.75, this value was 65%. Fig. 5(b) presents UV-Vis absorption spectra of bilayer P3HT/PCBM films of various compositions. The reference film [1 : 1 (bottom)/1 : 1 (top)] and the optimized bilayer film [1 : 0.25 (bottom)/1 : 1.75 (top)] displayed the same absorption behavior because their overall compositions were the same. Nevertheless, the imbalance of the charge transport properties in the device having the composition 1 : 1/1 : 1 allowed more space charge carriers to accumulate at the metal–organic interface, resulting in recombination of charge and decreased photocurrent generation.

Fig. 6 presents the current density–voltage (J–V) characteristics of bilayer devices having various bottom/top layer combinations. Table 2 summarizes the device parameters for all the devices prepared in this study. The device having a single-layer BHJ and the bilayer device having a P3HT/PCBM ratio of 1 : 1 in each layer exhibited efficiencies of 2.51 and 2.61%, respectively. The bilayer device in which the top layer had a P3HT/PCBM ratio of 1 : 1.75 and the bottom layer had a ratio of 1 : 0.25 exhibited the highest PCE (3.52%), with a short-circuit current (J_{SC}) of 11.67 mA cm^{-2}, a fill factor (FF) of 0.51, and an open-circuit voltage (V_{OC}) of 0.59. As expected, the presence of a graded concentration in the active layer can result in a higher PCE than that of the corresponding device without a graded concentration in the active layer. Thus, the vertical composition profile is an important factor for further optimization of device performance.

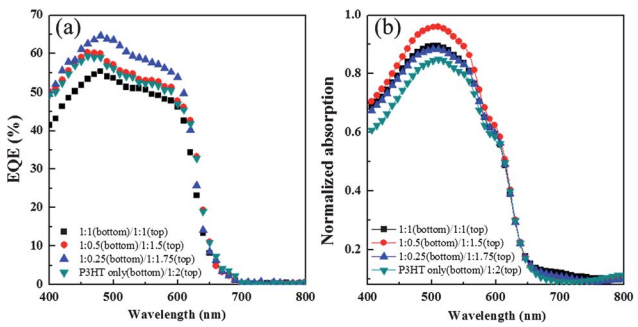

Fig. 5 (a) EQE spectra of devices and (b) UV-Vis absorption spectra of P3HT:PCBM films in bilayer structures with controlled P3HT/PCBM compositions. (■) The top layer (1 : 1 P3HT/PCBM ratio) transferred onto the bottom layer (1 : 1 P3HT/PCBM ratio); (●) the top layer (1 : 1.5 P3HT/PCBM ratio) transferred onto the bottom layer (1 : 0.5 P3HT/PCBM ratio); (▲) the top layer (1 : 1.75 P3HT/PCBM ratio) transferred onto the bottom layer (1 : 0.25 P3HT/PCBM ratio); (▼) the top layer (1 : 2 P3HT/PCBM ratio) transferred onto the 100% P3HT bottom layer.

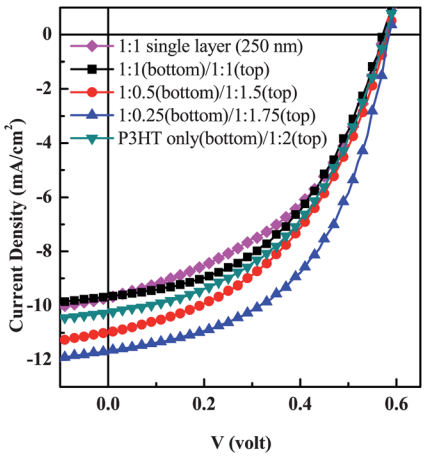

Fig. 6 The cell performance tested under AM 1.5 G (100 mW cm^{-2}) conditions for bilayer structures with various P3HT:PCBM compositions. (◆) Single layer (1 : 1 P3HT/PCBM ratio); (■) the top layer (1 : 1 P3HT/PCBM ratio) transferred onto the bottom layer (1 : 1 P3HT/PCBM ratio); (●) the top layer (1 : 1.5 P3HT/PCBM ratio) transferred onto the bottom layer (1 : 0.5 P3HT/PCBM ratio); (▲) the top layer (1 : 1.75 P3HT/PCBM ratio) transferred onto the bottom layer (1 : 0.25 P3HT/PCBM ratio); (▼) the top layer (1 : 2 P3HT/PCBM ratio) transferred onto the 100% P3HT bottom layer.

Table 2 Performance parameters of devices with BHJ and P3HT/PCBM composition-controlled bilayer structures

Composition of P3HT and PCBM (bottom/top)	J_{SC}/mA cm^{-2}	V_{OC}/Volt	PCE (%)	FF
1 : 1 (BHJ)	9.69	0.58	2.51	0.45
1 : 1/1 : 1 (reference cell)	9.67	0.58	2.62	0.47
1 : 0.5/1 : 1.5 (bilayer)	10.95	0.58	2.87	0.45
1 : 0.25/1 : 1.75 (bilayer)	11.67	0.59	3.52	0.51
P3HT-only/1 : 2 (bilayer)	10.25	0.58	2.76	0.46

To further demonstrate the application of stamping techniques for the preparation of organic electronics, we used the same method to also fabricate PLEDs with multilayer structures. Typically, a PLED structure consists of an anode, a layer of PEDOT:PSS, an emission layer (EL), and a cathode. Direct contact between the PEDOT:PSS layer and the conducting layer, due to the absence of an HTL and/or electron blocking layer (EBL) between the PEDOT:PSS and EL, is one of the reasons why PLEDs feature inefficient charge injection and quenching effects. The injection barrier between the PEDOT:PSS and EL layers is usually high, leading to a high driving voltage and, therefore, low power efficiency, especially for blue light-emitting materials, where the energy level of the highest occupied molecular orbital (HOMO) is very deep relative to the work function of PEDOT:PSS. It is also difficult to insert another organic layer between the PEDOT:PSS layer and the EL because the layer beneath often has a solubility similar to that of the EL in common organic solvents and will, therefore, be washed away while depositing the upper layer. Here, we used stamp-transfer processes to fabricate a bilayer polymer structure to improve PLED performances.

Fig. 7 presents the device performances of bilayer PLED structures with various thicknesses of the TFB layer and a fixed thickness of the blue EL sandwiched between the anode and cathode. The current efficiency and power efficiency of the PLEDs increased after incorporation of the TFB layer. It was found that devices with a thinner TFB layer have better *I–V–L* characteristics, and poorer efficiency resulted when the films were thicker than 50 nm. Devices with a 20 nm TFB layer have the best *I–V–L* characteristics, but devices with a 0.5 nm TFB layer have the highest current efficiency. The current efficiency is defined as the ratio of the brightness and the current density. The ratio is higher for the devices with a 0.5 nm layer of TFB than the ones with 20 nm. The real reason for this high ratio is unknown. It is most likely because of the optical effect due to the ultrathin layer of the TFB, resulting in the improvement at the interface, and avoiding the wave-guide loss at the same time.

We attribute two factors for the improved device performance after the addition of the TFB layer. First, the decrease of the energy barrier for the hole injection, due to the HOMO energy level (5.5 eV) of TFB being positioned between those of PEDOT (5.2 eV) and blue PF (5.8 eV), assisted charge injection into the EL. This improvement is evident in Fig. 7(a) and (b), with increased current density and brightness. Fig. 7(c) shows the TFB thickness dependences on the current efficiency, which can indicate the overall improvements resulted from the existence of the TFB layer. Second, the existence of the TFB layer prevented direct contact between the EL and the highly conductive PEDOT:PSS polymer blend, minimizing the possibility of exciton quenching or dissipation from the adjacent layer. This enhancement is evident in Fig. 7(d), with a lower efficiency roll-off at the stage of high current density relative to that of reference devices prepared without a TFB layer.

In addition, *IVL* characterization revealed that the effects of additional interface states on charge injection were fairly small relative to the improvements resulting from the decreased energy barrier between the HTL and LEL.

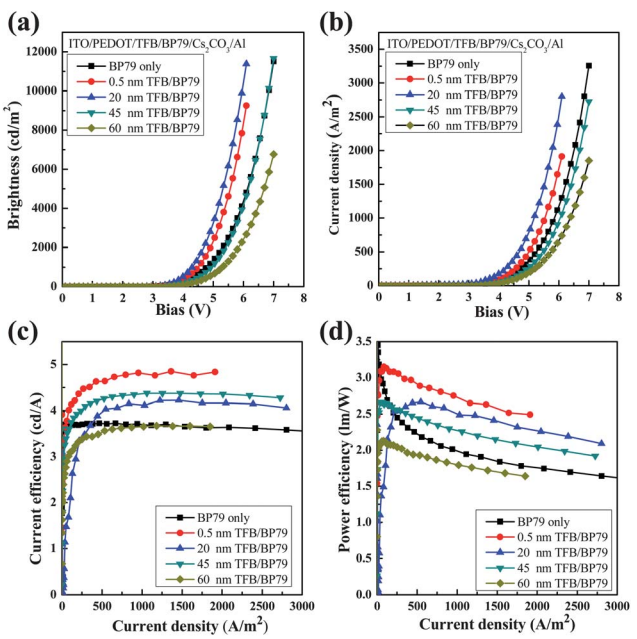

Fig. 7 (a) Brightness–*V* characteristics, (b) *J–V* characteristics, (c) current efficiency, and (d) power efficiency, plotted with respect to the current density for PLEDs featuring various TFB layer thicknesses.

Conclusions

We have demonstrated that organic solar cells possessing a P3HT-rich/PCBM-rich bilayer structure and multilayer light emitting devices can be fabricated through the use of the stamping process. Among our systems, the solar cell featuring a bilayer structure containing a P3HT-rich (1 : 0.25) bottom layer and a PCBM-rich (1 : 1.75) top layer exhibited the best PCE (3.52%). The better performance is contributed from the formation of inter-concentration gradient which is favorable to the charge transport. The charge mobility calculated from the SCLC model also indicates the concentration gradient within the film can lead to a much balanced charge transport ($\mu_e/\mu_h = 1.16$ for the device with a P3HT-rich (1 : 0.25) bottom layer and a PCBM-rich (1 : 1.75) top layer). When we applied a similar technique to the fabrication of PLEDs, the current efficiency of the device featuring a TFB interlayer increased by 27% (to 4.7 cdA^{-1}, from 3.7 cdA^{-1} for the device prepared without a TFB layer). Our results suggest that stamp-transfer processes not only provide another route for the production of multiple-layer polymer devices but also increase the flexibility of structure design with potentially improved device performance.

Acknowledgements

The authors are grateful to the Academia Sinica research program on nanoscience and nanotechnology for financial support.

References

1 F. C. Chen, S. C. Chien and G. L. Cious, *Appl. Phys. Lett.*, 2010, **97**, 103301.
2 X. Gong, M. Tong, Y. Xia, W. Cai, J. S. Moon, Y. Cao, G. Yu, C. L. Shieh, B. Nilsson and A. J. Heeger, *Science*, 2009, **325**, 1665.
3 R. H. Friend, R. W. Gymer, A. B. Holmes, J. H. Burroughes, R. N. Marks, C. Taliani, D. D. C. Bradley, D. A. Dos Santos, J. L. Brédas, M. Lögdlund and W. R. Salaneck, *Nature*, 1999, **397**, 121.
4 P. K. H. Ho, J.-S. Kim, J. H. Burroughes, H. Becker, F. Y. Li, T. M. Brown, F. Cacialli and R. H. Friend, *Nature*, 2000, **404**, 481.
5 J. J. M. Halls, C. A. Walsh, N. C. Greenham, E. A. Marseglia, R. H. Friend, S. C. Moratti and A. B. Holmes, *Nature*, 1995, **376**, 498.
6 S. H. Park, A. Roy, S. Beaupre, S. Cho, N. Coates, J. S. Moon, D. Moses, M. Leclerc, K. Lee and A. J. Heeger, *Nat. Photonics*, 2009, **3**, 297.
7 S. Su, E. Gonmori, H. Sasabe and J. Kido, *Adv. Mater.*, 2008, **20**, 4189.
8 S. Reineke, F. Lindner, G. Schwartz, N. Seidler, K. Walzer, B. Lüssem and K. Leo, *Nature*, 2009, **459**, 234.
9 M. Nakamura, C. Yang, E. Zhou, K. Tajima and K. Hashimoto, *ACS Appl. Mater. Interfaces*, 2009, **1**, 2703.
10 D. H. Wang, D. G. Choi, K. J. Lee, O. Park and J. H. Park, *Langmuir*, 2010, **26**, 9584.
11 F. C. Krebs, *Sol. Energy Mater. Sol. Cells*, 2009, **93**, 484.
12 K. H. Yim, Z. Zheng, Z. Liang, R. H. Friend, W. T. S. Huck and J. S. Kim, *Adv. Funct. Mater.*, 2008, **18**, 1012.
13 V. C. Tung, J. Kim, L. J. Cote and J. Huang, *J. Am. Chem. Soc.*, 2011, **133**, 9262.
14 J. Yang, R. Zhu, Z. Hong, Y. He, A. Kumar, Y. Li and Y. Yang, *Adv. Mater.*, 2011, **23**, 3465.
15 S. R. Tseng, S. C. Lin, H. F. Meng, H. H. Liao, C. H. Yeh, H. C. Lai, S. F. Horng and C. S. Hsu, *Appl. Phys. Lett.*, 2006, **88**, 163501.

16 J. H. Huang, Z. Y. Ho, T. H. Kuo, D. Kekuda, C. W. Chu and K. C. Ho, *J. Mater. Chem.*, 2009, **19**, 4077.
17 D. S. Germack, C. K. Chan, B. H. Hamadani, L. J. Richter, D. A. Fischer, D. J. Gundlach and D. M. DeLongchamp, *Appl. Phys. Lett.*, 2009, **94**, 233303.
18 A. Kumar, G. Li, Z. Hong and Y. Yang, *Nanotechnology*, 2009, **20**, 165202.
19 J. H. Huang, F. C. Chien, P. Chen, K. C. Ho and C. W. Chu, *Anal. Chem.*, 2010, **82**, 1669.
20 G. Zhao, Y. He and Y. Li, *Adv. Mater.*, 2010, **20**, 4355.
21 J. H. Huang, C. Y. Yang, Z. Y. Ho, D. Kekuda, M. C. Wu, F. C. Chien, P. Chen, C. W. Chu and K. C. Ho, *Org. Electron.*, 2009, **10**, 27.
22 C. J. Ko, Y. K. Lin and F. C. Chen, *Adv. Mater.*, 2007, **19**, 3520.
23 J. H. Huang, K. C. Li, D. Kekuda, H. H. Padhy, H. C. Lin, K. C. Ho and C. W. Chu, *J. Mater. Chem.*, 2010, **20**, 3295.
24 J. H. Huang, K. C. Li, F. C. Chien, Y. S. Hsiao, D. Kekuda, P. Chen, H. C. Lin, K. C. Ho and C. W. Chu, *J. Phys. Chem. C*, 2010, **114**, 9062.
25 J. H. Huang, C. M. Teng, Y. S. Hsiao, F. W. Yen, P. Chen, F. C. Chang and C. W. Chu, *J. Phys. Chem. C*, 2011, **115**, 2398.
26 D. S. Germack, C. K. Chan, B. H. Hamadani, L. J. Richter, D. A. Fischer, D. J. Gundlach and D. M. DeLongchamp, *Appl. Phys. Lett.*, 2009, **94**, 233303.
27 A. Kumar, G. Li, Z. Hong and Y. Yang, *Nanotechnology*, 2009, **20**, 165202.
28 J. H. Huang, F. C. Chien, P. Chen, K. C. Ho and C. W. Chu, *Anal. Chem.*, 2010, **82**, 1669.
29 S. S. V. Bavel, M. Barenklau, G. With, H. Hoppe and J. Loos, *Adv. Funct. Mater.*, 2010, **20**, 1458.
30 J. W. Jung, J. W. Jo and W. H. Jo, *Adv. Mater.*, 2011, **23**, 1782.
31 N. Wang, X. Liu and X. Liu, *Adv. Mater.*, 2008, **20**, 2211.
32 H. J. Schneider, L. Tianjun, N. Lomadze and B. Palm, *Adv. Funct. Mater.*, 2004, **14**, 615.
33 V. Shrotriya, G. Li, Y. Yao, T. Moriarty, K. Emery and Y. Yang, *Adv. Funct. Mater.*, 2006, **16**, 2016.
34 Y. L. Loo, R. L. Willett, K. W. Baldwin and J. A. Rogers, *Appl. Phys. Lett.*, 2002, **81**, 562.